Advanced Mathematical Models & Applications
Vol.7, No.3, 2022, pp.339-350

Jomard Publishing

NUMERICAL SIMULATION OF PROCESSES IN AUGER CONVERTER AS PART OF MOBILE ROBOTIC PLATFORM FOR 3D PRINTING*

Volodymyr Gritsyuk[1†], Igor Nevliudov[1], Murad Omarov[1], Oleksandr Tsymbal[1], Mykola Zablodskiy[2], Volodymyr Pavlysh[3]

[1]Department of Computer-Integrated Technologies, Automation and Mechatronics Kharkiv National University of Radio Electronics, Kharkiv, Ukraine
[2]Department of Electrical Engineering, Electromechanics and Electrotechnology National University of Life and Environmental Sciences of Ukraine, Kyiv, Ukraine
[3]Department of Electronics and Information Technology, Lviv Polytechnic National University, Lviv, Ukraine

Abstract. In the paper a numerical simulation of electromagnetic processes in the auger rotor of heat-electromechanical converter was carried out based on the results of calculating a field problem. To solve nonlinear differential equations in partial derivatives, the finite element method is used, which was implemented with the Comsol Multiphysics software and computing system. The performed quantitative analysis of the spatial distribution of the eddy current density, as well as the dissipated power density in the auger converter's rotor, makes possible to develop recommendations for choosing rational parameters and material heating modes. The obtained results will help improve the efficiency and cost-effectiveness of a mobile robotic platform for 3D printing of large-scale structures by improving the design of the extruder assembly auger.

Keywords: Numerical simulation, 3D printing, finite element method, mobile robotic platform, electromechanical converter.
AMS Subject Classification: 6506.
†**Corresponding author:** Volodymyr, Gritsyuk, Department of Computer-Integrated Technologies, Automation and Mechatronics, Kharkiv National University of Radio Electronics, Nauky Ave. 14, Kharkiv, Ukraine,
Tel.: +380999485433, e-mail: *volodymyr.hrytsiuk@nure.ua*
Received: 16 July 2022; Revised: 23 September 2022; Accepted: 14 October 2022;
Published: 15 December 2022.

1 Introduction

3D printing is a trending technology of our time, and its use is increasing because it allows to reduce the cost of production. Additive manufacturing provides unique advantages in creating structures of complex shape, which are in great demand in the aerospace industry (Katz-Demyanetz et al., 2019), biomedicine (Yuk et al., 2020; Birbara et al., 2019), automotive industry (Jankovics & Barari, 2019) and other fields (Kolomiets et al., 2021; Wohlers et al., 2020). One of the 3D printing problems is that typical desktop printers are stationary and have limited workspace. Mobile 3D printing platforms solve this problem by allowing to move without restrictions (Sauter et al., 2021).

*__How to cite (APA)__: Gritsyuk, V., Nevliudov, I., Omarov, M., Tsymbal, O., Zablodskiy, M. & Pavlysh, V. (2022). Numerical simulation of processes in auger converter as part of mobile robotic platform for 3D printing. *Advanced Mathematical Models & Applications*, *7*(3), 339-350.

In addition to the design freedom, additive manufacturing has great potential in the construction industry, as well as in the production and repair of road surfaces. For example, employees of the Massachusetts Institute of Technology in Keating, et al. (2018) presented a large-scale digital construction platform (DCP) for sensing, analysis and digital production in any place. The second version of DCP used an electric tracked vehicle as a platform and was used to extrude foam when pouring walls, which is similar to the block construction method. In Tiryaki et al. (2019), the authors developed a mobile printing system consisting of two robotic manipulators on a mobile base that prints cement objects of a sufficiently large size. Researchers at the Institute of Advanced Architecture of Catalonia have presented an idea for mobile 3D printing that uses three separate systems to print architectural structures using cement (Hall, 2016).

In accordance with the concept of "self-repairing cities" (Jackson et al., 2018; Johansson, 2016), a fleet of autonomous vehicles and drones will scan roads for cracks and repair them before potholes appear. By detecting a crack in the road, a 3D printer robot can place asphalt in the crack to repair it, all within a minute. This approach can be taken at night to avoid road closures that could severely disrupt traffic. The device is based on a desktop RepRap-printer Mendel 90, but equipped with a special extruder and high-temperature photopolymer nozzle. Printing is performed with bituminous chips with millimeter-sized particles, poured into a hopper, heated and forced through a nozzle using an auger. The extruder assembly has an internal heating sleeve. The pellets are softened as they pass through the auger due to the rise in temperature due to the action of the heating resistors, which causes the liquid bitumen to flow out of the nozzle as shown in Fig. 1, a. Stepper motors, temperature, gradient and auger speed are controlled by simple electronics connected to a PC (Fig. 1, b).

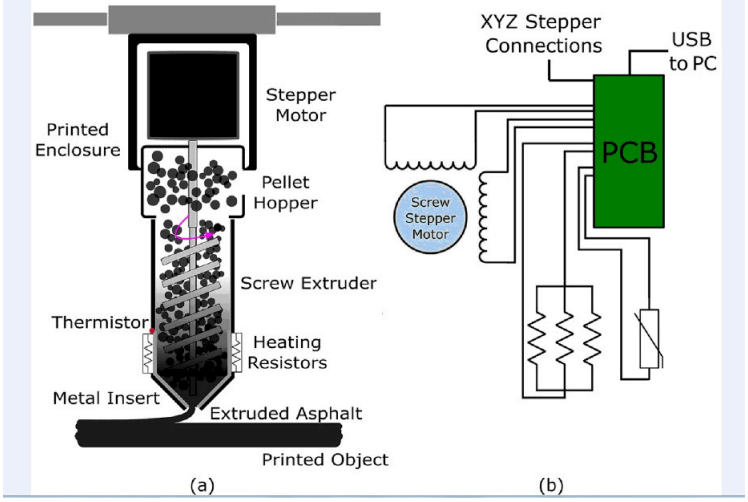

Figure 1: System design (Jackson et al., 2018): the extruder design (a), the control electronics (b)

The improved mechanical properties are a function of temperature, which is likely due to microstructural changes in the asphalt. This leads to the formation of fibers that bridge the cracks, which increases the toughness. Through experimentation, the authors found that temperatures between $125B^0C$ and $135B^0C$ are optimal for producing continuous asphalt extrusion with a constant line width.

3D printing technology for large-scale structures can be improved by combining an electric motor, auger extruder, and a heater in one package. This will provide not only savings in mass and size, but also a significant increase in the efficiency and reliability of the system due to functional integration and full use of the dissipative energy component. The need for additional heat sources will disappear, and the auger rotor, completely immersed in the material, is able to transfer maximum thermal and mechanical energy to it.

Thus, in order to increase the efficiency, economy and versatility of devices that provide transportation, mixing, pressing and heating operations, it is important to use them as links

in the technological chain. As an alternative to the above approaches, a mobile robotic platform equipped with auger heat-electromechanical converter (HEMC) is proposed. The proposed converter uses an external auger rotor, which simultaneously performs the functions of an induction motor rotor, a heating element, an actuator and a protective housing (Fig. 2). Therefore, taking into account the "useful" losses of the electromagnetic system, the efficiency of heat-electromechanical converters for technological purposes increases to 98-99

The auger HEMC uses the principle of self-regulation in energy conversion, according to which the distribution of thermal and mechanical energy into useful flows is carried out in accordance with the value of the sliding, which depends on the ratio of the electromagnetic moments of the HEMC motor and brake modules. When the stator winding of the motor module is connected to a voltage source, a rotating magnetic field is created, under the influence of which eddy currents (EC) are induced in the adjacent area of the outer ferromagnetic rotor. As a result, an asynchronous electromagnetic torque is formed. The main mode can be considered the opposite direction of rotation of the fields, in which the braking module works when sliding $s_b r > 1$, i.e. in electromagnetic braking mode.

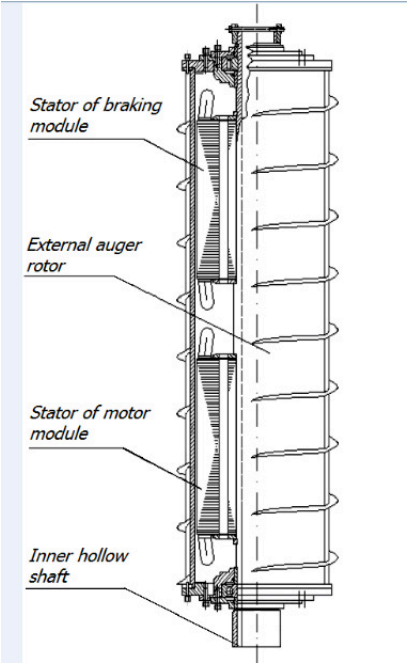

Figure 2: Constructive scheme of auger heat-electromechanical converter

2 Materials and methods

The study of the EC distribution induced in electrically conductive media is of practical interest for a wide range of industrial applications. EC in vacuum chambers, motor cores, high-speed magnets and accelerating resonators cause a number of adverse effects. First of all, we are talking about heating the cores and electrically conductive structural elements and, accordingly, reducing the overall efficiency of devices. At the same time, the assessment of heat releases that occur in conductors during the EC flow is important for various devices, such as induction furnaces, devices for melting, soldering, etc.

For example, in Aubert et al. (2012) due to the presence of rotor windows of a controlled induction motor, its EC within the active length of the machine will be directed mainly in the axial direction, which ensures an increase in the electromagnetic torque, efficiency and power factor. However, the obtained conclusions are formulated on the basis of an analytical solution for the EC density distribution of the rotor. Therefore, to improve the accuracy of calculations

and reduce development time, it is required to create improved three-dimensional mathematical models and efficient design algorithms.

Similarly, when developing of auger HEMC, it is necessary to perform a quantitative analysis of the EC density distribution and the dissipated power density in order to develop recommendations for choosing rational parameters and modes of heating the material.

Traditional methods and approaches to the calculation and analysis of processes in HEMC, taking into account the specificity of functioning, do not provide the necessary reliability of the results. Methods that provide high reliability of calculations are field and circuit-field methods of analysis, which are invariant to the nature of the electromagnetic connections of the object of study, take into account the real geometry and properties of materials. Circuit-field methods are used in the analysis of dynamic modes of operation of electromechanical converters.

The use of field methods of analysis makes it possible to carry out refined studies of the parameters, characteristics and operating modes of the HEMC, taking into account the design features and operating modes that cannot be reliably analyzed by traditional methods. The use of field methods is especially important for electromechanical converters operating in difficult conditions. During the electromechanical transformation of energy in the HEMC, a single force physical field arises, the separate components of which are the fields of electromagnetic, thermal and mechanical quantities. In the study of electromechanical converters, numerical methods for calculating the field are widely used, taking into account the geometry and saturation of the cores, among which the finite element method is especially progressing. According to the finite element method, the study area is divided into sections. The solution of differential equations is reduced to the solution of an algebraic system of equations relating the value of the vector potential of the field at the nodal points obtained by dividing into sections. The method of conductivities of toothed contours is widely used, according to which the full field of the machine is considered, taking into account its change in time during the mutual movement of the toothed cores. Electromagnetic processes are calculated by jointly solving a system of differential equations written in matrix form for the circuits of an electrical circuit, including the windings of the machine and external electrical circuits.

The greatest accuracy of the analysis is ensured when calculating a three-dimensional problem. This becomes possible when taking into account most of the physical effects that are more deeply manifested under conditions of full reproduction of the geometry of the device. The solution of a system of equations describing a three-dimensional electromagnetic and temperature field at any time for any spatial point of the model can only be implemented by numerical methods. These methods are widely used in modern multiphysics simulation software packages Cedrat Flux, Comsol Multiphysics, Ansys and others.

For a preliminary assessment of the efficiency of using auger HEMC as part of mobile robotic platforms for industrial 3D printing, it is necessary to analyze the EC distribution in a ferromagnetic rotor as the main sources of heat generation. This will provide important information for predicting the optimum temperature, gradient, and rotational speed of the auger extruder. In turn, the listed values will determine the mechanical properties of the material at the output of the device.

A highly accurate simulation approach based on 3D numerical analysis will allow better understanding and prediction of phenomena that are difficult and sometimes impossible to evaluate experimentally. To achieve the goal, the mathematical model presented in Zablodskiy et al. (2019, 2020) was used. In this work, a three-dimensional modification of the finite element model, which is implemented within the framework of the Comsol Multiphysics software and computing system, has been embodied. The means of analyzing the results of calculations of this particular complex make it possible to obtain comprehensive information about the processes occurring in the object under study. At the same time, Comsol Multiphysics is one of the most tested and available software products that implement the finite element method.

In the general case, the non-linear magnetic system of the auger HEMC consists of several

ferromagnetic bodies with non-linear physical properties of materials surrounded by a magnetic-linear medium. The electromagnetic field at each point of the studied area is determined by the magnetic induction vectors B of the magnetic field intensity H of the electric displacement D and the electric field intensity E.

The system of Maxwell's equations for the electromagnetic field vectors in all areas of the auger HEMC is a mathematical model of non-linear magnetic system with a current densities distribution. In the practice of electromechanical converters fields calculations, to bring the Maxwell's equations system to a form more convenient for solving, the vector magnetic potential $\vec{A}$ is often used, which is determined by the expression:

$$rot\vec{A} = \vec{B}. \tag{1}$$

Based on the Maxwell's equations, in media with non-linear magnetic characteristics, when using the vector magnetic potential, an equation can be written, which describes the electromagnetic field for randomly time-varying distributed alternating currents, including eddy currents in massifs.

Ampere's circuital law with account of (1) and the properties of the media

$$rot(\frac{1}{Oj}\vec{A}) = \vec{J}_{eddy} + \vec{J}_{ext}, \tag{2}$$

where $\mu = \mu_0 \Delta\mu_r$ is the absolute magnetic permeability; μ_0 is a magnetic permeability in vacuum; μ_r is a relative magnetic permeability; $\vec{J}_{eddy}$ is the eddy currents density; $\vec{J}_{ext}$ is the extraneous currents density. Using the scalar magnetic potential ϕ, the expression for the eddy currents density can be written:

$$\vec{J}_{eddy} = \gamma \left(-\frac{\partial \vec{A}}{\partial t} \right) + grad\varphi, \tag{3}$$

where γ is a specific electrical conductivity. Having substituted the expression for the eddy currents density into equation (2) and accepting the calibration conditions $divA = \mu\gamma\varphi$, let us perform the vector transformations and obtain the differential equation of the electromagnetic field in the partial derivatives according to the vector magnetic potential:

$$rot\left(\frac{1}{\mu} rot\vec{A}\right) - \gamma\frac{\partial \vec{A}}{\partial t} - \gamma\left(\vec{\nu} \times rot\vec{A}\right) = -\vec{J}_{\exp}, \tag{4}$$

where $\vec{\nu}$ is a velocity vector of the electrically conducting medium movement relative to the magnetic field source. For the case when the magnetic field varies in harmonic law, the equation (4) takes the form:

$$rot(\frac{1}{\mu} rot\vec{A}) - j\omega\gamma\vec{A} - \gamma\vec{\nu} \cdot (rot\vec{A}) = -\vec{J}_{ext}, \tag{5}$$

where ω is the angular frequency of the magnetic field changes. For non-conducting areas, the Poisson's equation is valid:

$$rot(\frac{1}{\mu} rot\vec{A}) = -\vec{J}_{ext}. \tag{6}$$

The solution of lengthy equations of the field in the numerical calculations of three-dimensional models is accompanied by significant difficulties. From the point of view of optimizing the hardware costs, it is expedient to perform the numerical calculation of a quasi-stationary electromagnetic field using the equation for the rotor coordinate system, since there is no convection component related to the rotor rotation relative to the coordinate system. Simplification of the equation (5), through the exclusion of the convection term, does not affect the approach to solving the problem, however, it contributes to the solution convergence, which enables to implement

practically the algorithm of numerical calculation. In the case of using a rotor coordinate system, the rotor remains motionless. Then, in the equation (5), it is necessary to accept the conditions:

$$\omega = \omega_1 \cdot s, \omega_R = 0, \nu_x = \nu_y = 0, \tag{7}$$

where ω_1 is the angular frequency of the stator field rotation; s is a rotor sliding; ω_R is the angular frequency of the rotor rotation; $\nu_{x,y}$ is a components of the velocity vector of the electrically conducting medium relative to the magnetic field source. Finally, the equation (5) can be written as:

$$rot(\frac{1}{\mu} rot\vec{A}) - j\omega_1 s\gamma\vec{A} = -\vec{J}_{ext}. \tag{8}$$

If in two-dimensional problems one component of $\vec{A}$ vector describes two components of the magnetic field, then, all three components should be considered in three-dimensional problems. The vector equation (8) for a three-dimensional magnetic field is equivalent to three equations:

$$\frac{\partial}{\partial x}\frac{1}{\mu}\frac{\partial A_x}{\partial x} + \frac{\partial}{\partial y}\frac{1}{\mu}\frac{\partial A_x}{\partial y} + \frac{\partial}{\partial z}\frac{1}{\mu}\frac{\partial A_x}{\partial z} - j\omega_1 s\gamma A_x = -J_x,$$

$$\frac{\partial}{\partial x}\frac{1}{\mu}\frac{\partial A_y}{\partial x} + \frac{\partial}{\partial y}\frac{1}{\mu}\frac{\partial A_y}{\partial y} + \frac{\partial}{\partial z}\frac{1}{\mu}\frac{\partial A_y}{\partial z} - j\omega_1 s\gamma A_y = -J_y,$$

$$\frac{\partial}{\partial x}\frac{1}{\mu}\frac{\partial A_z}{\partial x} + \frac{\partial}{\partial y}\frac{1}{\mu}\frac{\partial A_z}{\partial y} + \frac{\partial}{\partial z}\frac{1}{\mu}\frac{\partial A_z}{\partial z} - j\omega_1 s\gamma A_z = -J_z,$$

where $J_{x,y,z}$ is the components of the vector of extraneous currents density. Equation (8) is supplemented by boundary conditions. At the external boundaries of the computational domain (the three-dimensional model shell), a zero value of the vector magnetic potential is set (Dirichlet condition)

$$\vec{A} = 0. \tag{9}$$

The boundary condition (9) stipulates the accepted assumption that there are no magnetic fluxes leakage into the outer space through the considered boundaries. At the interface between media with different magnetic properties, the condition of normals equality to the boundary of the components of the magnetic induction vector and the tangent components of the magnetic field vector intensity is used (Neumann condition)

$$\vec{B}_{n1} = \vec{B}_{n2}, \vec{H}_{\tau 1} = \vec{H}_{\tau 2}. \tag{10}$$

Let us set the dependences of the media parameters on the spatial coordinates. Magnetic permeability as a function of magnetic field intensity for ferromagnetic media of the studied system in a matrix form:

$$[\mu_r] = \begin{bmatrix} \mu_{rx} & 0 & 0 \\ 0 & \mu_{ry} & 0 \\ 0 & 0 & \mu_{rz} \end{bmatrix}, \tag{11}$$

where $\mu_{rx,ry,rz}$ is a relative magnetic permeability along the x, y, z axes, respectively. The conductivity matrix for conducting media has the form:

$$[\gamma] = \begin{bmatrix} \gamma_x & 0 & 0 \\ 0 & \gamma_y & 0 \\ 0 & 0 & \gamma_z \end{bmatrix}, \tag{12}$$

where $\gamma_{x,y,z}$ is the electrical conductivity along the x, y, z axes, respectively. The basis for the numerical calculation of the three-dimensional quasi-stationary electromagnetic field of the auger HEMC is the partial differential equation (8), which is reducible to the algebraic equations system with respect to the target values of the vector magnetic potential at the nodes of the

finite element mesh. The vector magnetic potential is calculated based on the condition of the minimum of energy functional:

$$F = \int\limits_V \left[\frac{\partial}{\partial x}\frac{1}{\mu}\frac{\partial \overrightarrow{A}}{\partial x} + \frac{\partial}{\partial y}\frac{1}{\mu}\frac{\partial \overrightarrow{A}}{\partial y} + \frac{\partial}{\partial z}\frac{1}{\mu}\frac{\partial \overrightarrow{A}}{\partial z}\right] dxdydz + \\ + \int\limits_V j\omega\gamma \left|\overrightarrow{A^2}\right| dxdydz + \int\limits_V \overrightarrow{J}\,\overrightarrow{A}\, dxdydz. \tag{13}$$

Based on the results of calculating the distribution of the vector magnetic potential, the values of magnetic induction, induced EC and losses are calculated. The results of calculating the three-dimensional EC distribution are presented on the rotor part of the motor module. The three-dimensional geometry of the model is shown in Fig. 3 and consists of the following calculated sections: a hollow outer rotor, a geared stator magnetic circuit, an air gap and a stator winding.

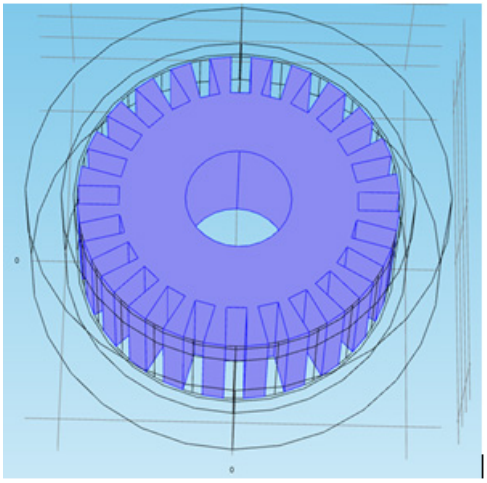

Figure 3: 3D geometry of auger heat-electromechanical converter model

The angular frequency of rotor rotation is defined as the frequency of the field sources in accordance with conditions (7) for the rotor coordinate system. The field sources on the right-hand side of equation (8) are specified by the external current density in the sections of stator grooves according to the three-phase winding connection scheme. Complex values of current density in phases of stator winding:

$$\begin{aligned} \overrightarrow{J}_A &= I_m \cdot u_g / S_g, \\ \overrightarrow{J}_B &= -I_m[\cos(-2\pi/3) - j\sin(-2\pi/3)] \cdot u_g / S_g, \\ \overrightarrow{J}_C &= -I_m[\cos(-4\pi/3) - j\sin(-4\pi/3)] \cdot u_g / S_g, \end{aligned} \tag{14}$$

where I_m is the amplitude of the current in the stator phase (data of the physical model); u_g is a number of effective conductors in the groove; S_g is a sectional area of the groove. The specific electrical conductivity of the rotor material was taken in accordance with the reference data, taking into account the average temperature with a working sliding for the motor module s = 0.88. The nonlinearity of the magnetic properties of the massive rotor and the stator core is taken into account by setting the corresponding magnetization curves.

3 Results and discussion

The solving problem result of three-dimensional EC distribution is shown in Fig. 4 in the form of a single transverse section of a hollow rotor at $s = 0.88(n_2 = 90rpm)$. The cut is made in the edge zone of the hollow cylinder, and the value of the z-component EC density is determined by shading of different colors and intensities.

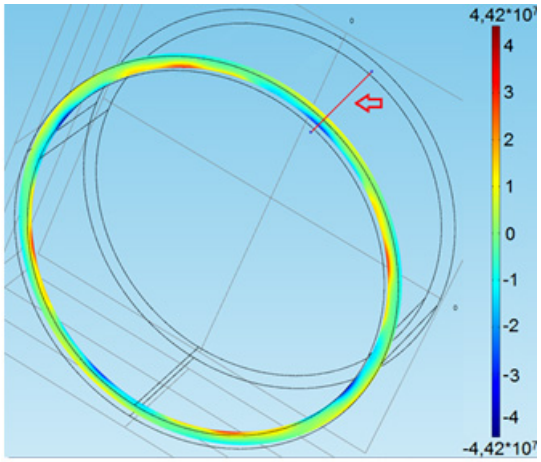

Figure 4: Distribution of the eddy current density (z-component) in the cross section of the outer hollow rotor at $s = 0.88(A/m^2)$

The same figure shows a line along which a section of the rotor wall is made, shown in Fig. 5. For comparison, in Fig. 6, 7 shows a cross section of the rotor and a cut along its wall at $s = 0.08(n_2 = 690rpm)$.

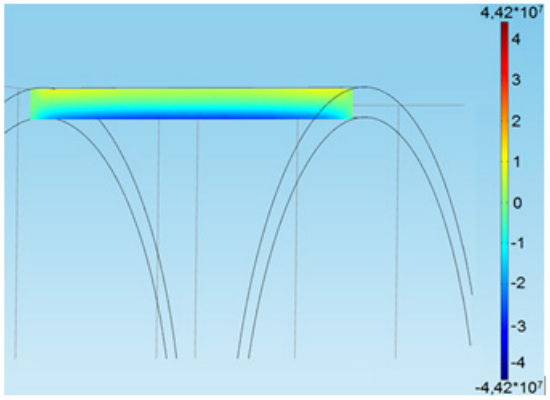

Figure 5: Distribution of the eddy current density (z-component) in the cross section of the outer hollow rotor at $s = 0.88(A/m^2)$

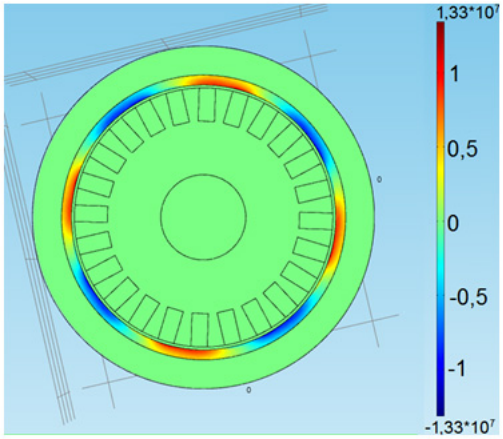

Figure 6: Distribution of the eddy current density (z-component) in the cross section of the outer hollow rotor at $s = 0.08(A/m^2)$

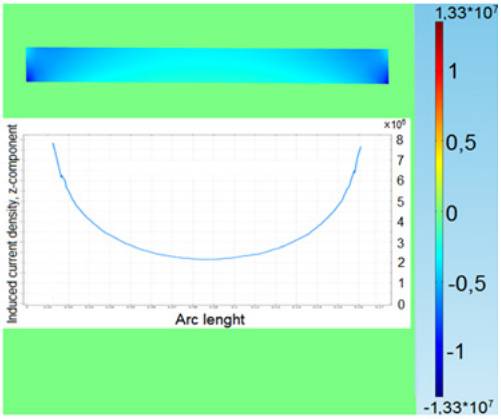

Figure 7: Distribution of the eddy current density (z-component) in the wall of the outer hollow rotor at $s = 0.08(A/m^2)$

In this mode, the frequency of the current in the rotor is only 4 Hz, however, the displacement of EC to the edges of the cylinder becomes noticeable. The maximum value of the z-component of EC density is 3.3 times lower than in the case for $s = 0.88$, and constitutes $13.3A/mm^2$. The largest value of the normal component of the EC density slightly exceeds the maximum value $(4.42A/mm^2)$ z-components for $s = 0.88$. In the three-dimensional picture of the normal component distribution (Fig. 8), internal areas of a higher EC density are noticeable, which are due to the presence of an internal tooth-groove structure of the stator. Those main source of thermal power is a layer of the inner surface of the rotor (4-5 mm), facing the source of the electromagnetic field.

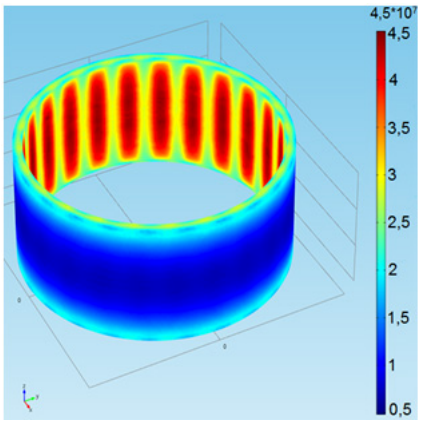

Figure 8: Distribution of the eddy current density (normal component) in the outer hollow rotor at $s = 0.88(A/m^2)$

The distribution pattern of the dissipated power density has a similar character, taking into account all types of losses in the rotor (Fig. 9). Predominantly, the dissipated power density on the outer surface of the rotor is within $(10.5 - 20)\Delta 10^6 W/m^3$. A significant difference in the dissipated power density between the inner and outer surfaces of the rotor under operating conditions is not critical. The thermal energy of the rotor is actively transferred to the surrounding material, and the temperature gradient in the direction of the thickness of the cylinder wall will remain small (Zablodskiy et al., 2017, 2014).

It should be noted that the nature of the dissipated power density distribution in the rotor changes significantly with an increase in the field frequency, which affects the quality of the thermal effect on the material. This is due to a change in the configuration of the EC flow contours, probably due to a decrease in the electromagnetic field penetration depth, as well

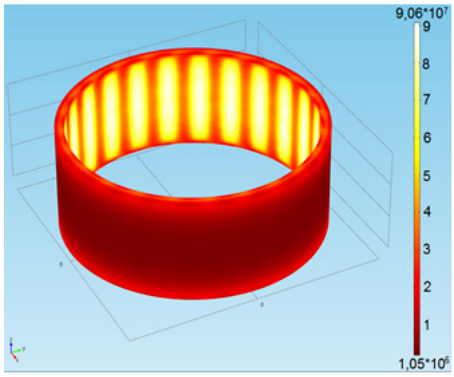

Figure 9: Dissipated power density distribution in the outer hollow rotor at $s = 0.88(W/m^3)$

as the influence of the edge effect. Fig.10 shows a spatial picture of the instantaneous EC distribution in the form of streamlines for the operating mode at $s = 0.88$.

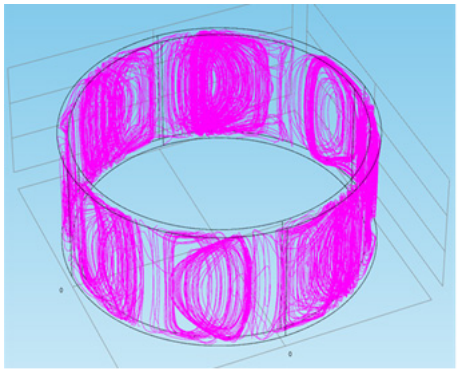

Figure 10: Eddy current distribution in the form of streamlines in the outer hollow rotor at $s = 0.88$

The presented data differ from the classical distribution in the form of rectangular and elliptical contours, obtained taking into account the influence of the edge effect (Aubert et al., 2012; Mirzaei et al., 2019). The complexity and variety of spatial configurations of the EC circuits in the HEMC rotor lead to the need to perform a separate detailed analysis.

4 Conclusion

Numerical simulation of electromagnetic processes in the rotor of auger heat-electromechanical converter was carried out based on the results of calculating a field problem. To solve nonlinear differential equations in partial derivatives, the finite element method was used, which was implemented with the Comsol Multiphysics software and computing system. A quantitative analysis of the spatial distribution of the eddy currents density, as well as the dissipated power density in the rotor of the auger converter, has been carried out, which makes possible to develop recommendations for choosing rational parameters and modes of heating the material. The obtained results will help improve the efficiency and cost-effectiveness of a mobile robotic platform for 3D printing of large-scale structures by improving the design of the auger extruder assembly. This is achieved by combining the electric motor, auger extruder and heater in one housing.

References

Annenkov, A., Sizikov, S. & Shiyanov, A. (2018). Asynchronous motor with perforated hollow rotor. *Energetika. Proceedings of CIS Higher Education Institutions and Power Engineering Associations*, *61*(2), 129-140.

Aubert, G., Jacquinot, J.F. & Sakellariou, D. (2012). Eddy current effects in plain and hollow cylinders spinning inside homogeneous magnetic fields: Application to magnetic resonance. *The Journal of Chemical Physics*, *137*(15), 154-201.

Birbara, N.S., Otton, J.M. & Pather, N. (2019). 3D modelling and printing technology to produce patient-specific 3D models. *Heart, Lung and Circulation*, *28*(2), 302-313.

Hall, N. (2016). *IAAC: Minibuilders, small robots with big ambitions*. 3D Printing Industry.

Jackson, R.J., Wojcik, A. & Miodownik, M. (2018). 3D printing of asphalt and its effect on mechanical properties. *Materials & Design*, *160*, 468-474.

Jankovics, D., Barari, A. (2019). Customization of automotive structural components using additive manufacturing and topology optimization. *IFAC-PapersOnLine*, *52*(10), 212-217.

Johansson, A. (2016). *3D printing robot may be the solution to potholes*. PSFK.

Katz-Demyanet, A., Popov Jr, V.V., Kovalevsky, A., Safranchik, D. & Koptioug, A. (2019). Powder-bed additive manufacturing for aerospace application: Techniques, metallic and metal/ceramic composite materials and trends. *Manufacturing review*, *6*.

Keating, S., Spielberg, N.A., Klein, J. & Oxman, N. (2014). Version digital construction platform: a compound arm approach. *Robot. Fabr. Archit. Art. Des.*, *4*, 99-110.

Kim, K.K., Ivanov, S.N. (2009). On the problem of determining speed-torque characteristics of thermal electromechanical converters. *Russian Electrical Engineering*, *80*(8), 459-465.

Kolomiets, A., Grobman, Y.J., Popov Jr, V.V., Strokin, E., Senchikhin, G. & Tarazi, E. (2021). The titanium 3D-printed flute: New prospects of additive manufacturing for musical wind instruments design. *Journal of New Music Research*, *50*(1), 1-17.

Mirzaei, M., Ripka, P., Vyhnanek, J., Chirtsov, A. & Grim, V. (2019). Rotational eddy current speed sensor. *IEEE Transactions on Magnetics*, *55*(9), 1-10.

Sauter, A., Nasirov, A., Fidan, I., Allen, M., Elliott, A., Cossette, M. & Singer, T. (2021). Development, implementation and optimization of a mobile 3D printing platform. *Progress in Additive Manufacturing*, *6*(2), 231-241.

Tiryaki, M.E., Zhang, X. & Pham, Q.C. (2019). Printing-while-moving: a new paradigm for large-scale robotic 3D Printing. In *2019 IEEE/RSJ International Conference on Intelligent Robots and Systems (IROS)*, 2286-2291.

Wohlers, T.T., Campbell, I., Diegel, O., Huff, R. & Kowen, J. (2020). Wohlers Report 2020: 3D printing and additive manufacturing global state of the industry. *Wohlers Associates*.

Yuk, H., Lu, B., Lin, S., Qu, K., Xu, J., Luo, J. & Zhao, X. (2020). 3D printing of conducting polymers. *Nature communications*, *11*(1), 1-8.

Zablodskiy, M., Gritsyuk, V., Rudnev, Y. & Brozhko, R. (2019). Three-dimensional electromagnetic field model of an auger electromechanicalconverter with an external solid rotor. *Mining of Mineral Deposits*, *13*(4), 99-106.

Zablodskiy, M., Gritsyuk, V., Rudnev, Y., Brozhko, R. & Tymofieieva, O. (2020). Analysis of 3D eddy current distribution in a hollow roto of an electromechanical converter. *In 2020 IEEE 40th International Conference on Electronics and Nanotechnology (ELNANO)*, 561-564.

Zablodskiy, N., Pliugin, V. & Gritsyuk, V. (2014). Submersible electromechanical transformers for energy efficient technologiesof oil extraction. *Progressive technologies of coal, coaled methane, and ores mining*, 223-227.

Zablodskii, N., Plyugin, V., Gritsyuk, V. & Grin, G.M. (2016). Polyfunctional electromechanical energy transformers for technological purposes. *Russian Electrical Engineering*, *87*(3), 140-144.

Zablodskiy, M., Zhiltsov, A., Kondratenko, I. & Gritsyuk, V. (2017). Conception of efficiency of heat electromechanicalcomplex as hybrid system. In *2017 IEEE First Ukraine Conference on Electrical and Computer Engineering (UKRCON)*, 399-404.